^{3}He scattering from ^{6}Li: A semimicroscopic approach

T. Sinha, Subinit Roy, and C. Samanta
Saha Institute of Nuclear Physics, 1/AF, Bidhan Nagar, Calcutta 700 064, India
(Received 17 December 1992)

Existing ^{6}Li (^{3}He, ^{3}He)^{6}Li elastic scattering data at 34, 50, 60, and 72 MeV have been reanalyzed with a microscopic potential in an elastic plus elastic triton-exchange model. The effects of the renormalization of the potential and the importance of the ^{3}He + t bound-state wave function are discussed.

PACS number(s): 24.50.+g, 25.55.−e, 25.55.Ci, 25.55.Hp

The real part of the optical potential in nucleus-nucleus collisions is generally estimated by the double folding model in which the effective nucleon-nucleon interaction is folded with the nuclear density distribution in nuclei [1]. This model is found to provide a satisfactory description of the foward angle data for nuclei with $A \geq 12$. However, for the ^{6}Li projectile it was noted that regardless of the target one must renormalize the folding model potential with a coefficient $N_R \sim 0.5$ to 0.7 [2]. For ^{6}Li + ^{6}Li scattering at 156 MeV, Sakuragi *et al.* showed that due to the low breakup threshold of ^{6}Li, the coupling between the elastic and the continuum states of ^{6}Li is responsible for this anomaly [3]. Similar results were found in the interaction of the ^{6}Li projectile with heavier nuclei [4,5] and at intermediate energies, the ^{6}Li projectile breakup effect was found to be less important [6]. It is therefore interesting to explore whether such renormalization is needed in the case of scattering of a composite projectile other than ^{6}Li from a ^{6}Li target and, if so, whether it has any energy dependence. The ^{6}Li(^{3}He,^{3}He)^{6}Li data available at 34, 50, 60, and 72 MeV [7] provide an excellent testing ground for such an investigation. A wide angular range covered by these data also gives the opportunity to find out the limitations, if any, of the folding model potential. In this work we have analyzed the above cited data in a semimicroscopic approach in which a recently formulated self-consistent microscopic potential was used. It was found that an energy-dependent renormalization constant is needed to fit the data.

The ground state of ^{6}Li is dominated by two overlapping configurations: $\alpha+d$ and ^{3}He$+t$ [8,9]. In the oscillator picture, the antisymmetrized wave functions for the lowest $T=0$ ^{6}Li states expressed as ^{3}He$+t$ and as $\alpha+d$ are mathematically equivalent [10]. This clustering aspect of ^{6}Li plays an important role in nuclear reactions and its effects can be seen even in the elastic scattering of d, ^{3}He, and α particles from ^{6}Li, which has a cluster substructure identical with these incoming projectiles [11–13]. From a phenomenological analysis Bragin *et al.* suggested [7] that the ^{3}He + ^{6}Li elastic scattering data at 34, 50, 60, and 72 MeV can be explained if a triton is exchanged between the ^{3}He projectile and the ^{3}He core of ^{6}Li. A coherent sum between the elastic and elastic triton transfer generated a back angle rise in cross section. The energy dependence of the extracted spectroscopic factor was attributed to the inaccuracy of the knowledge of the real part of the optical potential and it was suggested that the inclusion of other reaction mechanisms could change the values of the spectroscopic factors. In the above analysis (except for the 34 MeV data, which had very little back angle rise), two different sets of optical potential parameters were needed to generate the general features of the forward and backward angle data: a shallow potential at the entrance channel and a deeper potential at the exit channel. In an elastic plus core-transfer model a proper estimation of both the elastic part and the transfer part is crucial. A wrong estimation of the elastic part would lead to the use of a wrong spectroscopic factor to match the back angle rise. To remove the uncertainties of the optical potential parameters it is therefore desirable that a microscopic ^{3}He + ^{6}Li interaction potential should be used.

Recently, Kamal *et al.* [14] have calculated the real part of the ^{3}He + ^{6}Li potential in a consistent and self-congruous folding model taking a microscopic ^{6}Li internal wave function. This potential does not include any free parameters and it was found to provide an excellent fit to the ^{3}He + ^{6}Li elastic scattering data at 18 MeV taken up to $\theta_{\text{c.m.}} \sim 110°$ [15]. In this work, we reanalyzed the ^{6}Li(^{3}He,^{3}He)^{6}Li elastic scattering data of Bragin *et al.* [7] in a semimicroscopic approach using this potential

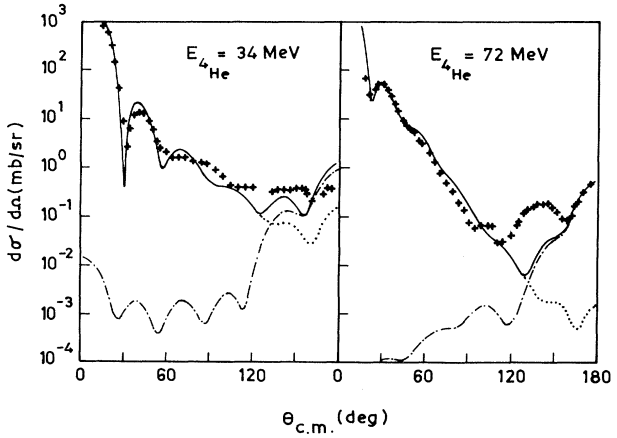

FIG. 1. The ^{6}Li(^{3}He,^{3}He)^{6}Li data at 34 and 72 MeV and semimicroscopic calculations with set C imaginary parameters, $N_R=1.0$ and $S=0.45$. The dotted curves are elastic, dash-dotted curves are transfer, and solid curves are elastic plus elastic triton transfer.

and the microscopic ^{3}He+t bound-state wave function of Lovas *et al.* [16]. For the imaginary part of the potential we used the imaginary parameters obtained from the phenomenological analysis of Bragin *et al.* We tested the effects of changing these imaginary parameters. To obtain the best fit to the forward angle data at 34 and 72 MeV (with $N_R=1.0$) a minor readjustment of the imaginary potential strength was needed. The corresponding imaginary parameters are given as set C in Table I. Incidentally, a good fit to the 50 and 60 MeV data could not be achieved by varying the imaginary potential strength keeping $N_R=1.0$. The pure elastic scattering formalism was found to be inadequate to explain the back angle rise of the data (Fig. 1). This limitation of the folding model potential is encountered because the cluster exchange phenomenon is not incorporated in the microscopic potential of Kamal *et al.* [14]. Following the prescription of Bragin *et al.*, we added a triton-exchange reaction mechanism explicitly to the elastic scattering. In this framework the scattering cross section $d\sigma/d\Omega$ is computed as

$$\frac{d\sigma}{d\Omega}=\tfrac{1}{4}|f_{\rm el}(\theta)+Sf_{\rm tr}(\pi-\theta)|^2 + \tfrac{3}{4}|f_{\rm el}(\theta)-Sf_{\rm tr}(\pi-\theta)|^2 \quad (1)$$

where $f_{\rm el}(\theta)$ is the amplitude of potential scattering and $f_{\rm tr}(\pi-\theta)$ is the amplitude of elastic transfer and S is the spectroscopic factor. The finite-range calculation was carried out using a slightly modified version of DWUCK5 [17]. To reproduce the back angle rise of the 72 MeV data a spectroscopic factor of 0.45 was needed (Fig. 1). Because of the large Q value of the ^{6}Li$\rightarrow^3$He+t ($Q=-15.796$ MeV) breakup, the triton cluster exchange

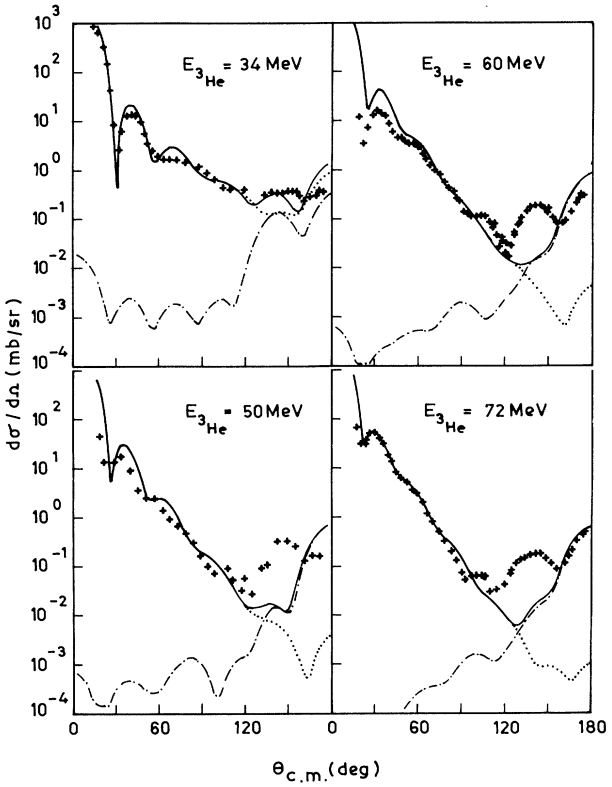

FIG. 2. The ^{6}Li(^{3}He,^{3}He)^{6}Li data at 34, 50, 60, and 72 MeV and semimicroscopic calculations with set A imaginary parameters, $N_R=1.0$, 0.84, 0.86, and 0.90, respectively, and $S=0.39$. The dotted curves are elastic, dashed-dotted curves are transfer, and solid curves are elastic plus elastic triton transfer.

TABLE I. Optical-potential parameters.

Reaction	E (MeV)	Set	$-V^a$ (MeV)	r_v (fm)	a_v (fm)	$-W^b$ (MeV)	r_W (fm)	a_W (fm)
^{3}He+^{6}Li	34.0	A	100.10 (1.00)	1.150	0.630	21.90 (27.00)	1.460	0.951
		B	100.10 (1.00)	1.150	0.630	21.90 (32.00)	1.460	0.951
		C	(1.00)			30.0	1.460	0.951
	50.0	A	91.77 (0.84)	1.150	0.650	32.11	1.460	0.843
		B	114.50 (1.00)	1.739	0.400	31.46 (32.50)	1.824	0.858
	60.0	A	90.20 (0.86)	1.150	0.644	27.70	1.460	0.830
		B	113.0 (1.00)	1.694	0.402	32.03 (33.0)	1.820	0.877
	72.0	A	87.50 (0.90)	1.150	0.632	27.16	1.460	0.830
		B	113.20 (1.00)	1.626	0.395	32.88	1.821	0.877
		C	(1.00)			30.0	1.460	0.830

[a] Normalization constant N_R for the microscopic potential is given in parentheses.
[b] The $-W$ values in parentheses are used in the microscopic calculations with set AB (Fig. 3).

model is expected to be more valid at a higher incident energy. Therefore we fitted the 72 MeV data first and then maintained the same spectroscopic factor for calculations at other energies.

A relatively better fit to the data was obtained (Fig. 2) using an energy-dependent renormalization constant ($N_R = 0.84$, 0.86, and 0.90 at 50, 60, and 72 MeV, respectively) keeping the imaginary part the same as set A of Bragin *et al.* (Table I). A fixed spectroscopic factor 0.39 was used in these calculations. These renormalization constants did not have much influence on the fit for angles up to $\theta_{\text{c.m.}} \sim 20^0$. Beyond this angle the slope of the curve was found to change with the change of normalization. The 60 MeV data at the extreme forward angles look unusually low compared to the data at other energies. This low cross section at the forward angles could not be reproduced by changing the normalization of the microscopic potential or by changing the imaginary potential parameters. This might be due to some error in the 60 MeV data near the extreme forward angles.

To compare our semimicroscopic analysis with the phenomenological analysis of Bragin *et al.* (Fig. 3), we repeated the calculations of Bragin *et al.* with the phenomenological bound-state wave function and potential parameter set A at the entrance channel and set B at the exit channel (Table I). The bound-state wave function in the phenomenological analysis was calculated for a Woods-Saxon potential with radius parameter $r_0 = 1.25$ fm and diffuseness parameter $a = 0.65$ fm as suggested by Bragin *et al.* Figure 3 shows the phenomenological calculations with $S^2 = 0.1$, 0.3, 0.4, and 0.45 at 34, 50, 60, and 72 MeV, respectively. The semimicroscopic calculations with the microscopic potential of Kamal *et al.* and bound-state wave function of Lovas *et al.* were also carried out with the imaginary parameter set A at the entrance channel and set B at the exit channel and a fixed spectroscopic factor 0.55. The semimicroscopic calculations were repeated with the bound-state wave function of Bragin *et al.* [7] along with $S^2 = 0.1$, 0.3, 0.4, and 0.45, but this combination produced an inferior fit in the backward hemisphere. This exhibits the importance of the proper choice of the bound-state wave function. It may be noted that the role of the bound-state wave function is particularly significant in a finite range calculation. Although a phenomenological bound-state wave function may reproduce the correct angular distribution of the data, if the structure is unrealistic, it would either overestimate or underestimate the cross sections leading to an incorrect spectroscopic factor. Since a considerable uncertainty exists in the spectroscopic factor for the ^{3}He+t substructure of ^{6}Li [10, 16, 18], we used the wave function of Lovas *et al.* [16] as well as those used by Bragin *et al.* [7] and Roos *et al.* [8]. A comparsion of these three normalized wave functions are shown in Fig. 4. We find that the wave functions of Refs. [7, 8] are almost

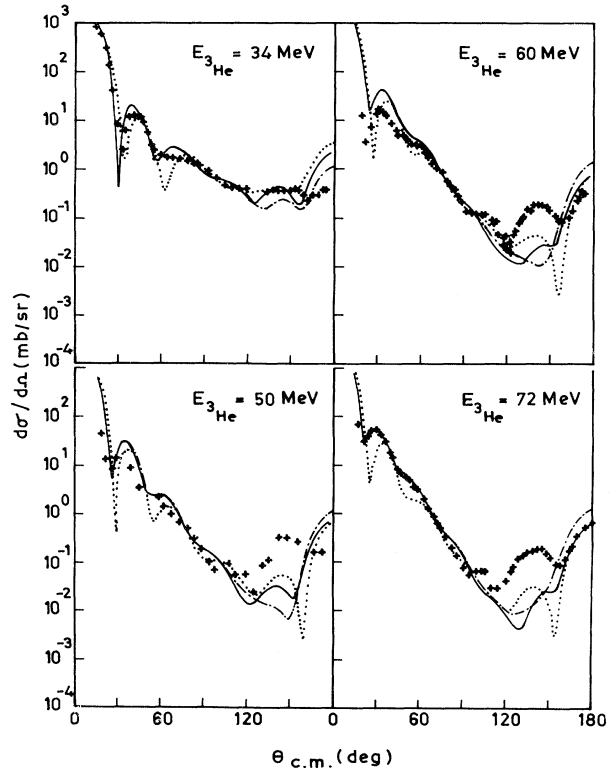

FIG. 3. The ^{6}Li(^{3}He,^{3}He)^{6}Li data at 34, 50, 60, and 72 MeV and calculations for elastic plus elastic triton transfer only. The solid curves are semimicroscopic calculations with set AB imaginary parameters, bound-state wave function of Ref. [16], and $S = 0.55$. The dash-dotted curves are semimicroscopic calculations with set AB imaginary parameters, bound-state wave function of Ref. [7] and $S^2 = 0.1$, 0.3, 0.4, and 0.45, respectively. The dotted curves are phenomenological calculations with set AB imaginary parameters, bound-state wave function of Ref. [7] and $S^2 = 0.1$, 0.3, 0.4, and 0.45, respectively.

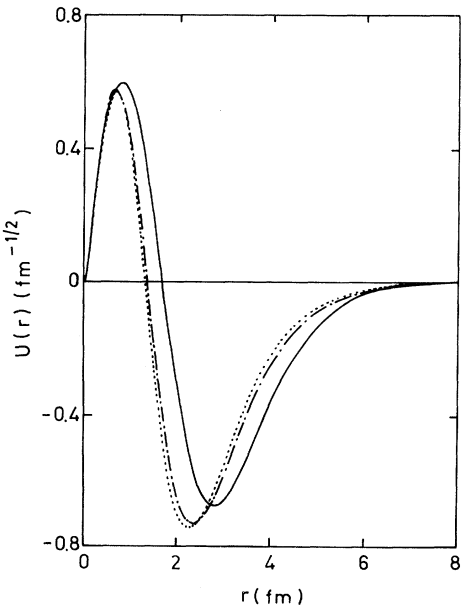

FIG. 4. Normalized ^{3}He+t bound-state wave functions. The solid curve is from Lovas *et al.* (Ref. [16]), the dotted one from Bragin *et al.* (Ref. [7]), and the dash-dotted one from Roos *et al.* (Ref. [8]).

identical whereas that of Ref. [16], which gives a better description of the data, is slightly different in amplitude and the first antinode is shifted towards larger radial direction.

The most interesting finding of this work is that the folding model potential for ^{3}He + ^{6}Li needs an energy dependent renormalization constant ($N_R = 1.0$, 0.84, 0.86, and 0.90 at 34, 50, 60, and 72 MeV, respectively) with the minimum value required at 50 MeV. One of the reasons for this energy dependence might be due to the fact that the microscopic potential of Kamal *et al.* has no implicit energy dependence. It could also be due to the limitations of the simple disorted wave Born approximation (DWBA) model used in this analysis. Because of the low $\alpha+d$ breakup threshold, the possible effects due to coupling to the continuum states cannot be ignored.

Another interesting finding is that, for any particular potential set (A, C, or AB), a unique energy-independent value of spectroscopic factor gives a satisfactory description of the back angle data. The value of this spectroscopic factor depends on the choice of imaginary potential parameters as well as on the N_R values which can be fixed by the forward angle fit. The extracted S in this analysis lies within $\sim$0.40 to 0.55 which is close to the latest theoretical prediction of 0.58 [16]. In the pure phenomenological analysis back angle fits comparable to the semimicroscopic analysis could be obtained with widely varying energy-dependent spectroscopic factors only. Our semimicroscopic calculations therefore provide a relatively more accurate description of both the elastic and the transfer part. However, the failure of this approach in the intermediate angular region points to some unresolved puzzle. In the region of intermediate angles where the cross sections from potential scattering and elastic cluster transfer are comparable, the structure of the angular distributions is determined by the complex interference of these processes and, in assessing the relative importance of interfering reaction mechanisms in fitting experimental data, it is pertinent to use an internally consistent microscopic potential which is as realistic as possible. Moreover we find that the cross section in the intermediate region is extremely sensitive to the choice of the bound-state wave function (Fig. 3). In this context, a microscopic ^{6}Li wave function calculated by extending the model state space with ^{3}He+t admixture incorporated, as mentioned in Ref. [18], as well as a microscopic ^{3}He + ^{6}Li interaction potential derived with this wave function, would be extremely useful.

The authors thank A. A. Ogloblin for providing us the data in tabular form and H. Rebel and S. K. Samaddar for helpful discussions.

[1] G. R. Satchler and W. G. Love, Phys. Rep. **55**, 183 (1979).
[2] G. R. Satchler, Phys. Rev. C **22**, 919 (1980).
[3] Y. Sakuragi, M. Kamimura, S. Micek, H. Rebel, and H. J. Gils, Z. Phys. A **322**, 627 (1985).
[4] Y. Sakuragi, M. Yahiro, and M. Kamimura, Prog. Theor. Phys. **70**, 1047 (1983).
[5] H. Nishioka, J. A. Tostevin, R. C. Johnson, and K. I. Kubo, Nucl. Phys. **A415**, 230 (1984).
[6] Y. Sakuragi, Phys. Lett. B **220**, 22 (1989).
[7] V. N. Bragin, N. T. Burtebaev, A. D. Duisebaev, G. N. Ivanov, S. B. Sakuta, V. I. Chuev, and L. V. Chulkov, Yad. Fiz. **44**, 312 (1986) [Sov. J. Nucl. Phys. **44**, 198 (1986)].
[8] P. G. Roos, D. A. Goldberg, N. S. Chant, R. Woody III, and W. Reichart, Nucl. Phys. **A257**, 317 (1976).
[9] D. F. Jackson, in *Clustering Phenomena in Nuclei,* edited by K. Wildermuth and P. Kramer (Vieweg, Braunschweig, 1983), Vol. 3, p. 157.
[10] K. Wildermuth and Y. C. Tang, *A Unified Theory of the Nucleus* (Academic, New York, 1977).
[11] V. I. Chuev, V. V. Davidov, B. G. Novatskii, A. A. Ogloblin, S. B. Sakuta, and D. V. Stepanov, J. Phys. (Paris) **C6**, 163 (1971).
[12] K. A. Gridnev and A. A. Ogloblin, Fiz. Elem. Chastits At. Yad. **6**, 393 (1975) [Sov. J. Part. Nucl. **6**, 158 (1976)].
[13] D. Bachelier, M. Bernas, J. L. Boyard, H. L. Harney, J. C. Jourdain, P. Radvanyi, M. Roy-Stephan, and R. Devries, Nucl. Phys. **A195**, 361 (1972).
[14] M. Kamal, V. T. Voronchev, V. E. Kukulin, V. M. Krasnopolsky, Y. Nakao, and K. Kudo, J. Phys. G **18**, 379 (1992).
[15] R. W. Givens, M. K. Brussel, and A. J. Yavin, Nucl. Phys. **A187**, 490 (1972).
[16] R. G. Lovas, A. T. Kruppa, R. Beck, and F. Dickmann, Nucl. Phys. **A474**, 451 (1987).
[17] P. D. Kunz, computer code DWUCK5 (unpublished).
[18] A. Csótó and R. G. Lovas, Phys. Rev. C **46**, 576 (1992).